



Research paper

Isouronium and *N*-hydroxyguanidinium derivatives as Cell growth inhibitors: A comparative studyAmila Kahvedžić-Seljubic^a, Seema-Maria Nathwani^b, Daniela M. Zisterer^b, Isabel Rozas^{a,*}^a School of Chemistry, Trinity Biomedical Science Institute, Trinity College Dublin, 152-160, Pearse St., Dublin 2, Ireland^b School of Biochemistry and Immunology, Trinity Biomedical Science Institute, Trinity College Dublin, 152-160, Pearse St., Dublin 2, Ireland

ARTICLE INFO

Article history:

Received 29 September 2015

Received in revised form

16 March 2016

Accepted 17 March 2016

Available online 22 March 2016

Keywords:

DNA minor groove binders
 Isouronium diaromatic derivatives
 Hydroxyguanidinium diaromatic derivatives
 Thermal DNA denaturation
 Cell growth inhibition
 HL-60 cells
 Kelly cells
 Flow cytometry
 Apoptosis

ABSTRACT

Based on the results obtained from a computational study on the suitability of the isouronium and *N*-hydroxyguanidinium cations as hydrogen bond donors/acceptors, the DNA binding of a series of isouronium derivatives was assessed by DNA thermal denaturation experiments and compared to related *N*-hydroxyguanidines. Due to the poor DNA binding observed, the nature of the diaromatic linker was explored by preparing the corresponding amide-linked *bis*-isouronium derivative and measuring its DNA affinity. Next, the inhibitory effects of the isouronium derivatives on cell viability were evaluated in two different cancer cell lines providing IC₅₀ values in the range of 36.9–57.4 μM (HL-60, leukemia), and 17.3–33.9 μM (Kelly, neuroblastoma). These values are comparable to those previously found for the *N*-hydroxyguanidine series. Compounds with the –S– linker (**3**, **6**, and **10**) proved to be considerably active in the HL-60 cells and even more active in the Kelly cell line. No correlation was found between DNA minor groove binding and cell growth inhibition; hence, activity may depend on different modes of action. Further studies into the apoptotic potential of these compounds indicated that, besides inhibiting cell viability and proliferation, derivatives **9** and **10**, are significant apoptosis-inducers in both cell lines. Results obtained with HL-60 cells suggest that G₂/M arrest and subsequent apoptosis induced by compound **10** are associated with microtubular depolymerisation, loss of mitochondrial membrane potential and activation of the caspase cascade. Moreover, the effects of compound **10** on cell viability and apoptosis in two non-carcinogenic cell lines (NIH3T3 and MCF-10A) indicate none or minimal toxicity.

© 2016 Elsevier Masson SAS. All rights reserved.

1. Introduction

Compounds that specifically bind with high affinity into the minor groove of DNA have shown potential for the treatment of diseases at a DNA level and, for this reason, minor groove binders (MGBs) have been widely studied as antibacterial, antiprotozoal, antitumor and antiviral agents [1–5]. The structures of these compounds often contain amidine-like functionalities (amidine, guanidine, 2-aminoimidazole, imidazole). Examples include

pentamidine, used for the treatment of African trypanosomiasis [6] or *Pneumocystis carinii* pneumonia and leishmaniasis [7]; berenil, used for animal trypanosomiasis [8]; pyrrole-imidazole polyamides, some of which have exhibited antitumor activity [9]; distamycin-based *bis*-alkenyl polyamides which have potent activity against Gram-positive bacteria by formation of very specific hydrogen bonds (HBs) [10]; or analogues of imidazoline-pyrrole based MGBs that have shown efficacy in human papilloma virus strains *in vitro* [11].

Over the past 15 years we have prepared a large number of symmetric and asymmetric di-aromatic guanidinium and 2-aminoimidazolium derivatives as DNA MGBs with potential cytotoxic/antiparasitic activity (Fig. 1) [12–17].

Considering the encouraging results obtained with these guanidine-based families, we prepared additional analogues incorporating isouronium and *N*-hydroxyguanidinium functionalities. Our aim was to probe the cationic binding to the DNA minor

Abbreviations List: DNA, deoxyribonucleic acid; AT, adenine-thymine base pair; MGB, minor groove binder; MP2, second order Møller-Plesset calculation; HB, hydrogen bond; CD, circular dichroism; NMR, nuclear magnetic resonance; IR, infrared; HRMS, High resolution mass spectrometry; st, salmon testes; SPR, surface plasmon resonance; ΔT_m , change in thermal melting temperature; P/D, phosphate/drug; RU, response units; IC₅₀, concentration required for 50% inhibition.

* Corresponding author.

E-mail address: rozasi@tcd.ie (I. Rozas).

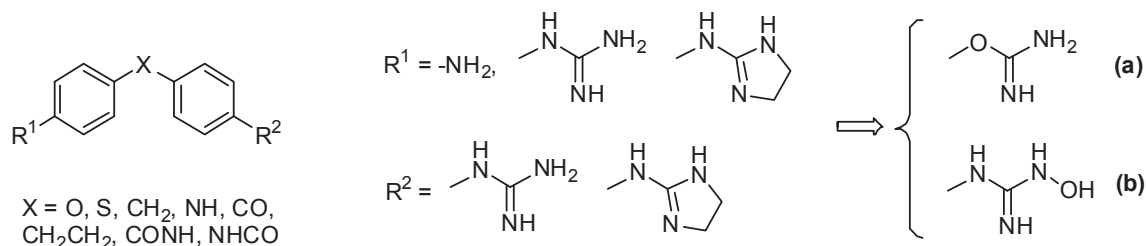


Fig. 1. Generic structure of guanidine-like derivatives developed by Rozas and coworkers [12–17] and structure of the isourea (a) and *N*-hydroxyguanidine (b) functionalities.

groove by introducing an O atom (HB acceptor) connecting the aromatic ring to the amidinium group (isouronium) or by adding an OH functionality (HB donor/acceptor) to the guanidinium cation (*N*-hydroxyguanidinium). We hypothesised that by increasing the number of contacts within the minor groove, improved cytotoxic agents would result. Furthermore, a variety of biophysical measurements including DNA thermal denaturation, SPR, CD, LD and ITC were used to study their binding into the minor groove [6,7].

In particular, we have recently reported the preparation of a series of *bis-N*-hydroxyguanidine derivatives as potential MGBs, their biophysical properties as well as their cytotoxicity assessment [18]. We found that, even though, somewhat surprisingly, they exhibited poor DNA binding affinity, their ability as growth inhibitors in a number of human cancer cell lines was very promising. Despite the preparation of a series of *bis*-isouronium derivatives being previously reported by our group [19], their biophysical characteristics and, more importantly, their effect on cancer cell growth have not been previously discussed. In this article, we present the discussion of the biophysical and biochemical properties of the *bis*-isouronium derivatives in comparison with the related *bis-N*-hydroxyguanidine cationic systems in order to investigate whether the introduction of a HB acceptor in amidine-based cations has an effect on their DNA binding affinity and anticancer activity.

With this comparative aim, we also present a theoretical study of the strength of all the possible HBs formed by the guanidine, isourea and *N*-hydroxyguanidine cations with models of HB donors such as hydrogen fluoride [20] and HB acceptors such as formaldehyde [21] by means of second order Møller-Plesset (MP2 [22]) computations using aqueous solvation (PCM model [23]). Additionally, the results of the study of *bis*-isouronium 1–3 derivatives as DNA MGBs in comparison to the previously prepared *bis*-

hydroxyguanidiniums 4–7 [18] (Fig. 2) are presented. Some *mono*-isouronium derivatives (8–10, Fig. 2) are included as well in this study as relevant comparisons. Finally, considering that the amide functionality (CONH) is present in many MGBs [4,9,11,24] and that it considerably contributed to improving the binding affinity of our guanidine-like dicationic systems [15], the effect of the CONH linker in the isouronium and *N*-hydroxyguanidinium series was further explored. Thus, the amide-linked *bis*-isouronium was prepared and the DNA binding as well as the growth inhibition in different cell lines was assessed and compared to those of the previously prepared amide-linked guanidine-like dications.

2. Results and discussion

2.1. Theoretical study of isouronium and *N*-Hydroxyguanidinium cations

An important issue in the biological activity of a potential drug is its pK_a since the basicity of a compound determines the protonation state and hence the absorption of the compound. Accordingly, we have found that experimentally [25–27] and computationally [28] determined, the pK_a values of arylisouroniums (pK_a values of phenylisourea: 8.29 [27] and 4,4'-(*bis*-isourea)diphenylether: 10.4 [26]) and aryl-*N*-hydroxyguanidiniums (pK_a of phenyl-*N*-hydroxyguanidine: 8.9 [28]) are slightly lower than those of arylguanidiniums (pK_a values of phenylguanidine: 10.88 [27] and 4,4'-(*bis*-guanidine)diphenylmethane: 10.5 [25]) or aryl-2-aminoimidazoliums (pK_a values of phenyl-2-aminoimidazoline: 9.16 [27] and 4,4'-(*bis*-2-aminoimidazoline)diphenylmethane: 9.4 [25]). Thus, there is not a large difference between their pK_a values and consequently all cations would be equally protonated at physiological pH (7.4).

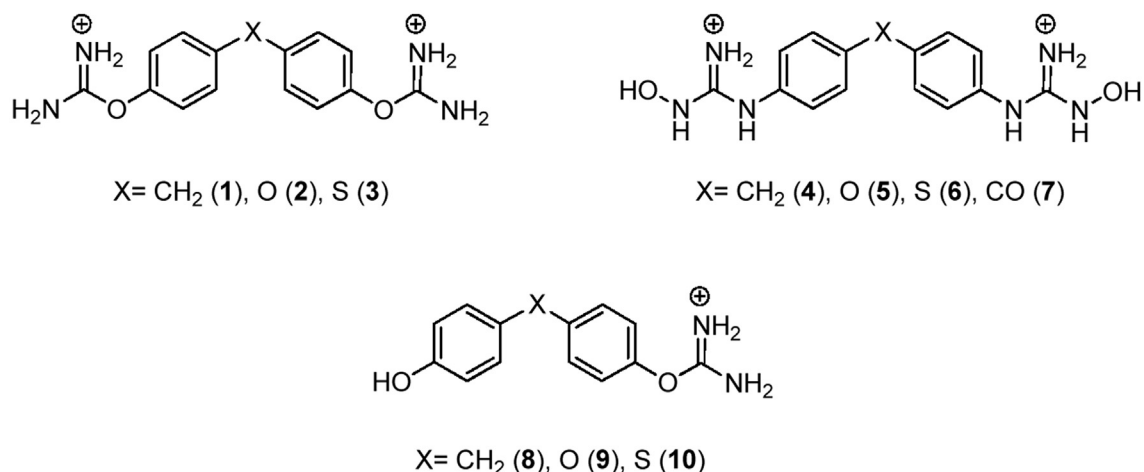


Fig. 2. *Bis*-isouronium (1–3), *bis-N*-hydroxyguanidinium (4–7) and *mono*-isouronium (8–10) derivatives here studied.

Moreover, the ability of the two cations to function as HB donors and/or acceptors could play an important role in the overall binding of the molecules into the DNA minor groove. Hence, we have theoretically explored all the possible HBs that these cations could form with widely used models of HB donors (HF [20]) and HB acceptors (H₂CO [21]) by means of DFT (M06-2X [29]) and second order Møller-Plesset (MP2 [22]) calculations using the 6-311++G** basis set [30] in a model of aqueous solvation (PCM [23]). Only MP2 results will be discussed here and M06-2X outcomes can be found in the Supporting Information (Tables S1 and S2). Whereas the guanidinium cation presents all HB donor amino groups, the isouronium cation presents two amino groups that can act as HB donors and an O atom that can act as a HB acceptor while the *N*-hydroxyguanidinium cation can form HBs as a donor through the three amino groups and the OH and it can accept HBs by means of the O atom in the hydroxyl group (Fig. 3). Hence, the corresponding models of HB acceptor and HB donor were located to interact with these groups forming single linear HBs [(O)(N)–H ⋯ OCH₂ or –(H/N)O ⋯ HF] or as three-centered systems where each HB acceptor atom simultaneously interacts with two HB donors. Optimisation of all these complexes yielded those shown in Fig. 4.

In the case of the complexes formed between the three cations and formaldehyde (Fig. 4a), all the complexes show strong interaction energies (Table S1, Supporting Information). In addition, all the contacts established show distances that are in agreement with HBs and were characterised by means of the AIM [31] analysis of the topology of the electron density surfaces, finding the corresponding bond critical points (BCP) with electron density characteristics in agreement with those of HBs [$\rho(\text{BCP}) \sim 10^{-3}$ a.u. and positive Laplacian of the $\rho(\text{BCP})$, see Tables S2 and S3, Supporting Information]. As can be seen in Fig. 4a, most of these optimised structures only showed bifurcated HBs where two HB donor groups (NH or OH) form a simultaneous interaction with the HB acceptor (the O atom of formaldehyde). The values obtained in terms of interaction energy and distances and electron density analysis of these contacts indicate that these HBs are very strong for the three families of compounds and that the strongest HBs formed are those between the OH of the *N*-hydroxyguanidinium and the HB acceptor.

In the case of the complexes with the model HB donor (HF, Fig. 4b), only the isouronium and *N*-hydroxyguanidinium cations are able to act as HB acceptors through the O atom. In the case of the *O*-phenylisouronium–HF complex (Fig. 4b), two interactions are observed; one between the O atom of the isouronium and the H of the HF molecule and a simultaneous interaction between an N–H of the isouronium and the F atom of HF that acts as a HB acceptor. In the case of the phenyl-*N*-hydroxyguanidine complex with HF, only one interaction is observed between the O of the hydroxyl group and the H atom of the HF molecule. As before, analysis of the interaction energies and distances as well as the electron density of these complexes (Tables S1 and S3, Supporting Information)

indicates that all of them are strong HBs.

From this theoretical study, we concluded that both the isouronium and *N*-hydroxyguanidinium cations have the potential to interact with DNA similar to the guanidinium cation since they can establish comparable HB interactions. Furthermore, the *N*-hydroxyguanidinium cation is more versatile both because of the number of interactions that it can form and its ability of forming the strongest O–H ⋯ O interaction that can be established among the compounds in this study. In addition, and as a notable difference compared to the guanidinium system, these O-containing cations can form extra HBs with DNA as HB acceptors.

2.2. DNA thermal denaturation experiments

Once the suitability of both types of O-containing cations in interacting with the DNA minor groove was established, DNA thermal denaturation was chosen as a suitable biophysical technique in order to assess DNA binding in these two series. Accordingly, using sequence unspecific salmon sperm DNA, a P/D of 10 and conditions previously established in the group [13–18], DNA thermal denaturation experiments were carried out for compounds 1–3 and 8–10 and ΔT_m values obtained (Table 1). These were compared to ΔT_m values of the related *N*-hydroxyguanidiniums 4–7 (Table 1). Despite the DNA binding of the isouronium derivatives being slightly better than that of the *N*-hydroxyguanidiniums, the ΔT_m values obtained were very low, indicating poor binding to DNA. However, comparing the ΔT_m values of the *bis*-isouroniums (1–3) to those of the corresponding *mono*-isouroniums (8–10), it is clear that dicationic systems are required for more optimal binding to DNA to be achieved (Table 1).

Thus, two conclusions were drawn from these experiments; firstly, that *bis*-cationic systems are required for optimal DNA binding. Secondly, considering the HB donor/acceptor ability of these two cations, it seems that the presence of more HB donor groups as in the *N*-hydroxyguanidine series does not improve the binding to DNA and, hence, other factors should be considered such as the geometry and nature of the linker between the aromatic systems.

2.3. Amide-linked derivatives

Considering the nature of the linker, we have previously observed that in the *bis*-guanidinium, *bis*-2-aminoimidazolinium and guanidinium/2-aminoimidazolinium series, the CONH linker highly improved the DNA affinity of these dicationic systems in comparison to more simple functionalities (CH₂, O, S) [15]. The amide group can partake in HB interactions both as a HB acceptor and donor, for example, in the case of netropsin, the CONH groups facilitate DNA binding by forming HBs with adjacent A:T base pairs. Similarly, modelling and crystal-structure studies showed that the

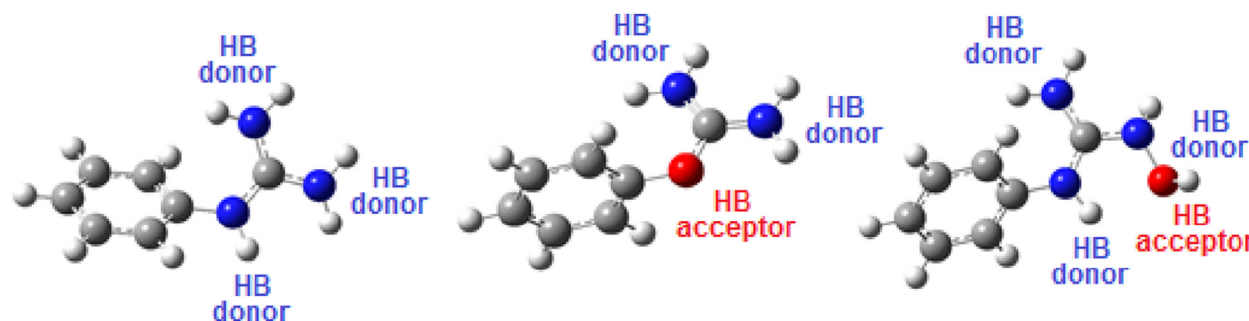


Fig. 3. HB donor and acceptor groups within phenylguanidinium (left), *O*-phenylisouronium (middle) and phenyl-*N*-hydroxyguanidinium (right) cations.

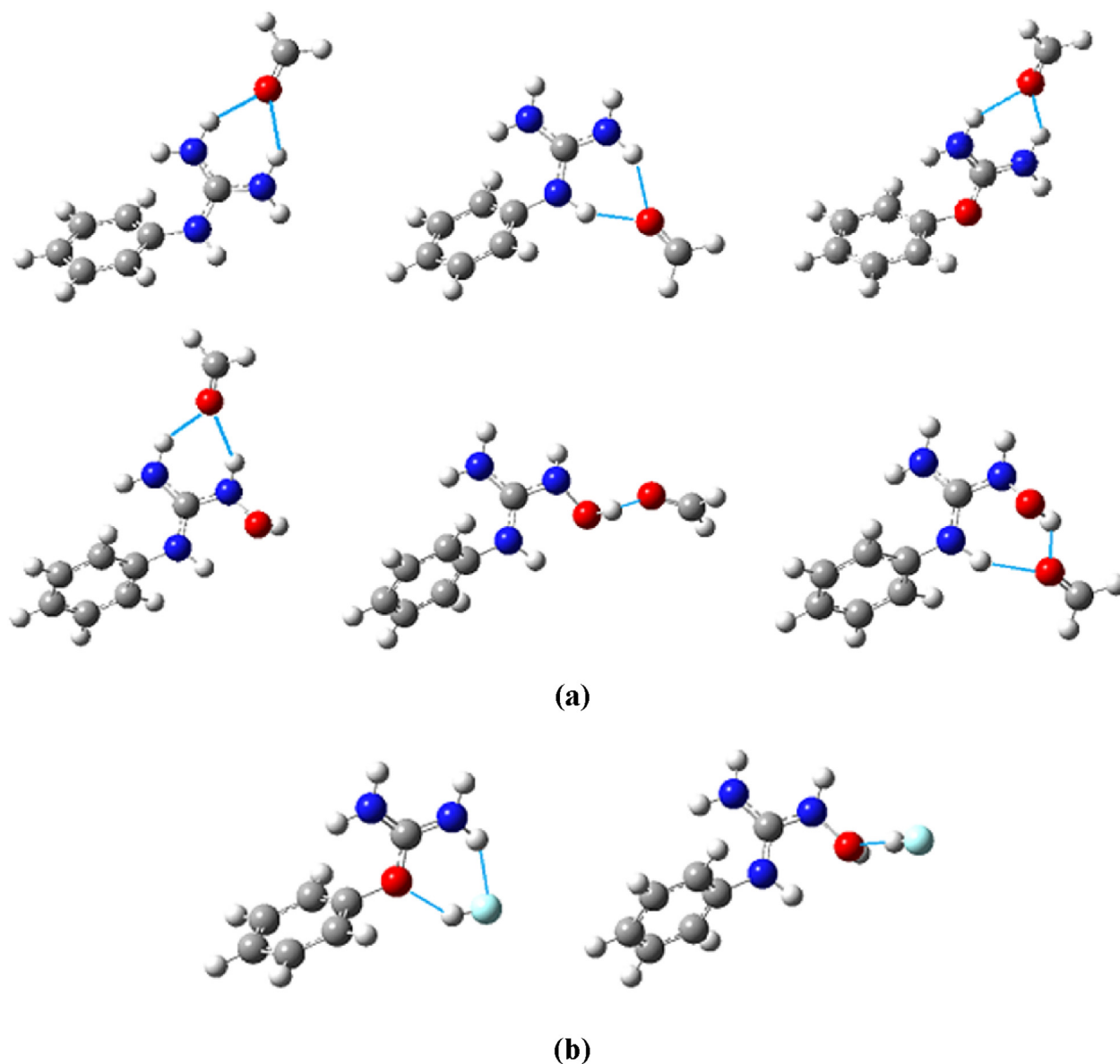


Fig. 4. Optimised structures (MP2/6-311++G**, PCM-water) of all the complexes formed between phenylguanidinium, phenylisouronium and phenyl-*N*-hydroxyguanidinium with (a) a model of a HB acceptor (formaldehyde) and (b) a model of a HB donor (hydrogen fluoride).

binding of distamycin A is partly attributed to HBs of its amide groups to adjacent A and T bases [32]. Therefore, we decided to prepare the corresponding *bis*-isouronium derivatives with a CONH linker (compound **11**, Scheme 1) and compare it to the previously prepared peptide linked *bis*-cations (including *bis*-*N*-hydroxyguanidiniums) to investigate whether DNA binding could be improved.

Our synthetic approach for the preparation of *bis*-isouronium derivatives requires a *bis*-hydroxy diaromatic derivative as starting material in order to install the amidinium group [19]. Considering that the corresponding amide-linked starting material is not commercially available, its preparation was achieved following the conditions described in the literature [33]. Thus, a DMF solution of 4-hydroxybenzoic acid chloride (recently prepared) was added drop-wise to 4-aminophenol dissolved in DMF along with a catalytic amount of DMAP, on ice under an inert atmosphere. Following a total reaction time of 20 h, the mixture was worked-up yielding the corresponding *bis*-hydroxy derivative **12**. It should be noted

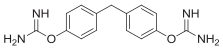
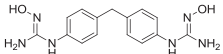
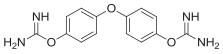
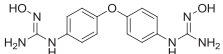
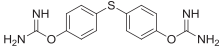
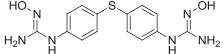
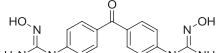
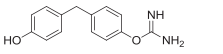
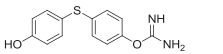
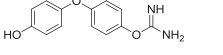
that when the reaction was performed in a 1:1 stoichiometry, only a 31% yield was obtained; however, using 3 equivs. of the aniline the yield was increased to 54%. This excess of starting material precipitated in EtOAc at work-up and was eliminated by filtration.

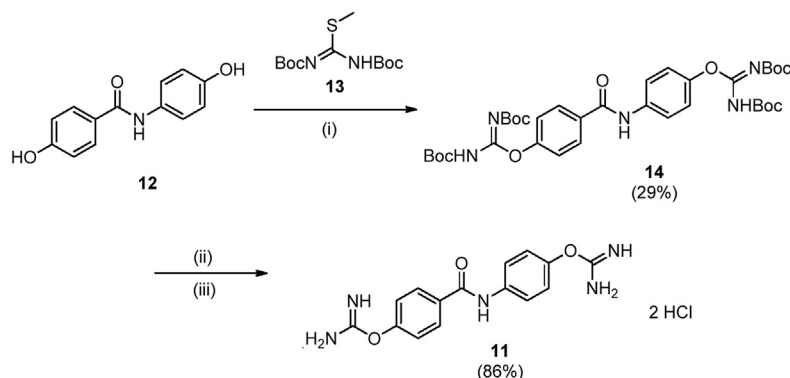
Next, the amidylation reaction was carried out taking into consideration previous procedures developed in our group [34]. Thus, compound **12** was reacted with 1,3-*bis*-(*tert*-butoxycarbonyl)-2-methyl-2-pseudothiourea (**13**) in the presence of HgCl₂/TEA at 0 °C and left stirring for 18 h at room temperature. The final product **14** was obtained in a 29% yield; this low yield can be accounted for by the electron-withdrawing nature of the amide linker and the formation of additional *mono*-substituted products. The corresponding hydrochloride salt (**11**) was generated in an 86% yield, by deprotection with TFA/DCM followed by treatment with Amberlyte resin (IRA400, Cl⁻) in water, work-up and reverse-phase chromatography (Scheme 1).

Slow evaporation from water afforded crystals of compound **11** and the resolved X-ray crystallographic structure is shown in Fig. 5.

Table 1

DNA thermal denaturation results obtained for amide-linked structures, isuronium and *N*-hydroxyguanidinium derivatives prepared by Rozas and coworkers in this and previous publications [6,7,9,10]. The increment in DNA thermal melting (ΔT_m , °C) is presented in unspecific salmon sperm DNA. DNA melting temperature in phosphate buffer (10 mM) was found to be 68 °C.

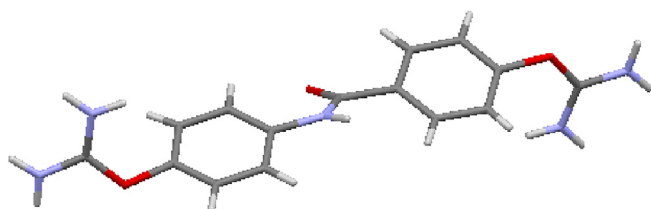
Compd.	Structure	$\Delta T_{m(SS)}$	Compd.	Structure	$\Delta T_{m(SS)}$
1		4	4 [18]		0
2		5	5 [18]		1
3		6	6 [18]		1
–	–	–	7 [18]		0
8		2	10		2
9		4	–	–	–



Reagents: (i) HgCl_2/TEA , 0 °C, overnight, rt. (ii) TFA/DCM. (iii) Amberlite resin (IRA400, Cl^-) in water

Scheme 1. Preparation of the amide-linked *bis*-isouronium salt (**11**).

In comparison to previously resolved *bis*-amidinium-like structures [19,22], derivative **11** does not possess a curved framework but adopts a more linear structure as a result of the planar nature of the amide bond, which is slightly rotated with respect to both aromatic rings. Regarding the cationic groups, they are not completely coplanar with the phenyl rings and adopt a slight curvature. Besides, as with the crystal of the O-linked *bis*-isouronium derivative (**2**) previously obtained [22], the presence of the coordinating Cl^- anions confirms that the structure is protonated in its solid state. Moreover, the bond length distances found in both isouronium cations are almost identical (C–O: 1.315, 1.322; C–N: 1.309, 1.333, 1.317, 1.304 Å), further implying that the positive charge is indeed

**Fig. 5.** Crystal structure of compound **11** obtained in the present work.

delocalised. Also, as before, these values are in the range of those found in the literature for differently substituted isouronium crystal structures [19,22].

Despite not having the typical curvature, compound **11** may still be considered a good candidate for binding into the DNA minor groove. On the one hand, as a dication, it retains the ability to bind electrostatically and, in addition, it can form HB bonds through the amidinium system. On the other hand, a study by Neidle and Wilson [35] showed that some linear compounds can indeed bind into the minor groove due to the presence of networked water molecules that add a degree of curvature to the linear systems.

Then, aiming to compare the ability of this *bis*-isouronium amide-linked derivative **11** with that of the corresponding amide-linked *bis*-guanidinium (**15**), *bis*-2-aminoimidazolium (**16**), asymmetric guanidinium/2-aminoimidazolium (**17**) and *bis*-*N*-hydroxyguanidinium (**18**) derivatives (see structures in Table 2), we carried out DNA thermal denaturation experiments with similar conditions to those used for the isouronium vs *N*-hydroxyguanidinium comparative study (*vide supra*). Additionally, our previously prepared amide-linked *mono*-guanidinium and 2-aminoimidazoline derivatives (**19** and **20** [15], see structures in Table 2) were also compared.

First, we confirmed that the presence of two cations is

Table 2
DNA thermal denaturation results obtained for amide-linked structures containing guanidinium, 2-aminoimidazolium, isouronium and *N*-hydroxyguanidinium cations. The increment in DNA thermal melting (ΔT_m , °C) is presented in unspecific salmon sperm DNA. DNA melting temperature in phosphate buffer (10 mM) was found to be 68 °C.

Compd.	Structure	$\Delta T_{m(SS)}$	Compd.	Structure	$\Delta T_{m(SS)}$
15 [15]		11	16 [15]		12.5
17 [15]		10	—	—	—
11		2	18 [18]		1
19 [15]		1	20 [15]		2

absolutely essential for optimal binding to DNA since the amide-linked mono-cations **19** and **20** gave as poor ΔT_m results (Table 2) as did the *mono*-isouroniums with different linkers (Table 1). In the case of the amide-linked dications, the introduction of a HB acceptor (-O-), as in the *bis*-isouronium **11**, seems to be detrimental to DNA binding and, hence, only HB donors would be recommended in the cationic moiety. This hypothesis may also validate the low ΔT_m of the *N*-hydroxyguanidinium **18** which, despite possessing an additional HB donor (-OH) also contains a HB acceptor (O atom of -OH) and hence, poorly binds to DNA. This result correlates to those found in the literature for *N,N*-dihydropentamidine, which, although proving to be as active as pentamidine in experimental mice as an antitrypanosomas agent [36], was found to be a poor DNA MGB [37]. Therefore, *N*-hydroxylation of pentamidine, as well as of *bis*-guanidinium diphenyl derivatives investigated in this study, results in an almost complete loss of DNA binding ability.

It seems clear that the introduction of HB acceptor groups in the cationic moieties of this type of MGB, despite the number of HB donor groups or the nature of the linker connecting the diaromatic system, results in poor binding to DNA.

2.4. Cell growth inhibition studies

Despite these poor DNA binding results, but based on the biological outcomes obtained for pentamidine and its dihydroxylated analogue [33], we performed cell viability studies with the *bis*-isouronium derivatives in two cancer cell lines (human Caucasian promyelocytic leukemia HL-60 and human neuroblastoma, Kelly) and the comparative results with the previous biochemical data for the *N*-hydroxyguanidinium series are presented in Table 3.

The HL-60 cell line is a valuable *in vitro* model which has been used in the literature for testing MGBs such as distamycin [38]. In our work, the *bis*- and *mono*-cationic isouroniums (**1–3**, **11** and **8–10**, respectively) were screened using the AlamarBlue[®] viability assay (redox dye which in its reduced form only in viable cells is fluorescent) and the results were compared to those previously reported for *bis*-*N*-hydroxyguanidiniums (**4–7**) [18]. Regarding the results obtained for the isouronium series (Table 3), compounds that produced sufficient inhibition (at least 50% cell viability reduction and IC₅₀ values of <100 μM) and those found to be inactive (IC₅₀ values of >100 μM) are presented in Fig. 6A.

The S-linked compound **3** was found to be the only active *bis*-

isouronium at the chosen concentration range and produced on average a 95.8% inhibition at 100 μM and an IC₅₀ of 57.4 ± 1.11 μM. Despite being weaker DNA binders than their di-cationic counterparts, the *mono*-isouroniums (**8–10**) were also assessed and surprisingly, **9** and **10** were found to be active. The S-linked derivative **10** produced an encouraging IC₅₀ (52.9 ± 1.45 μM) whilst the O-linked compound **9** was found to be more active with a lower IC₅₀ value (36.9 ± 1.15 μM).

Regarding the *N*-hydroxyguanidines, as previously reported [18], derivatives with CH₂, O and S linkers showed good inhibition of HL-60 cell growth (Table 3). Yet again, the best derivative of the group was found to be the S-linked compound (**6**) as indicated by the IC₅₀ values presented in Table 3.

Comparing the different families studied in the HL-60 cell line, we observed that all the compounds showing cell growth inhibitory activity (**3**, **4–6**, **9–10**) display better IC₅₀ values than the reference furamide (a known MGB as mentioned in the Introduction). Moreover, even though the inhibitory values of the *bis*-hydroxyguanidinium series (**4–7**) in this cell line are not the strongest overall, most of them were found to exhibit anti-proliferative effects with IC₅₀ values of 47.7–72.8 μM. This seems to suggest that the *N*-hydroxyguanidinium functionality is more beneficial for cell growth inhibition than the isouronium one.

Table 3

IC₅₀ values of *bis*- (**1–3**, **11**) and *mono*-isouroniums (**8–10**) and *bis*-hydroxyguanidiniums (**4–7**) in HL-60 and Kelly cell lines. Values are mean ± S.E.M. representatives of at least three independent experiments performed in triplicate.

Compd.	Cation ^a	Linker (X)	HL-60 IC ₅₀ (μM)	Kelly IC ₅₀ (μM)
1	Bis-Iso	CH ₂	>100	—
2	Bis-Iso	O	>100	—
3	Bis-Iso	S	57.4 (±1.1)	28.7 (±1.8)
11	Bis-Iso	NHCO	>100	>100
4	Bis-HydG	CH ₂	72.8 (±4.8) [18]	—
5	Bis-HydG	O	65.5 (±10.7) [18]	11.7 (±0.6) [18]
6	Bis-HydG	S	47.7 (±6.0) [18]	8.9 (±1.0) [18]
7	Bis-HydG	CO	>100 [18]	—
8	Mono-Iso	CH ₂	>100	—
9	Mono-Iso	O	36.9 (±1.5)	17.3 (±1.3)
10	Mono-Iso	S	52.9 (±1.5)	33.9 (±1.2)
Furamide			87.5 (±2.3) [18]	27.4 (±5.1) [18]

^a Cations: Bis-Iso = *bis*-isouronium; Mono-Iso = *mono*-isouronium; Bis-HydG = *bis*-*N*-hydroxyguanidinium.

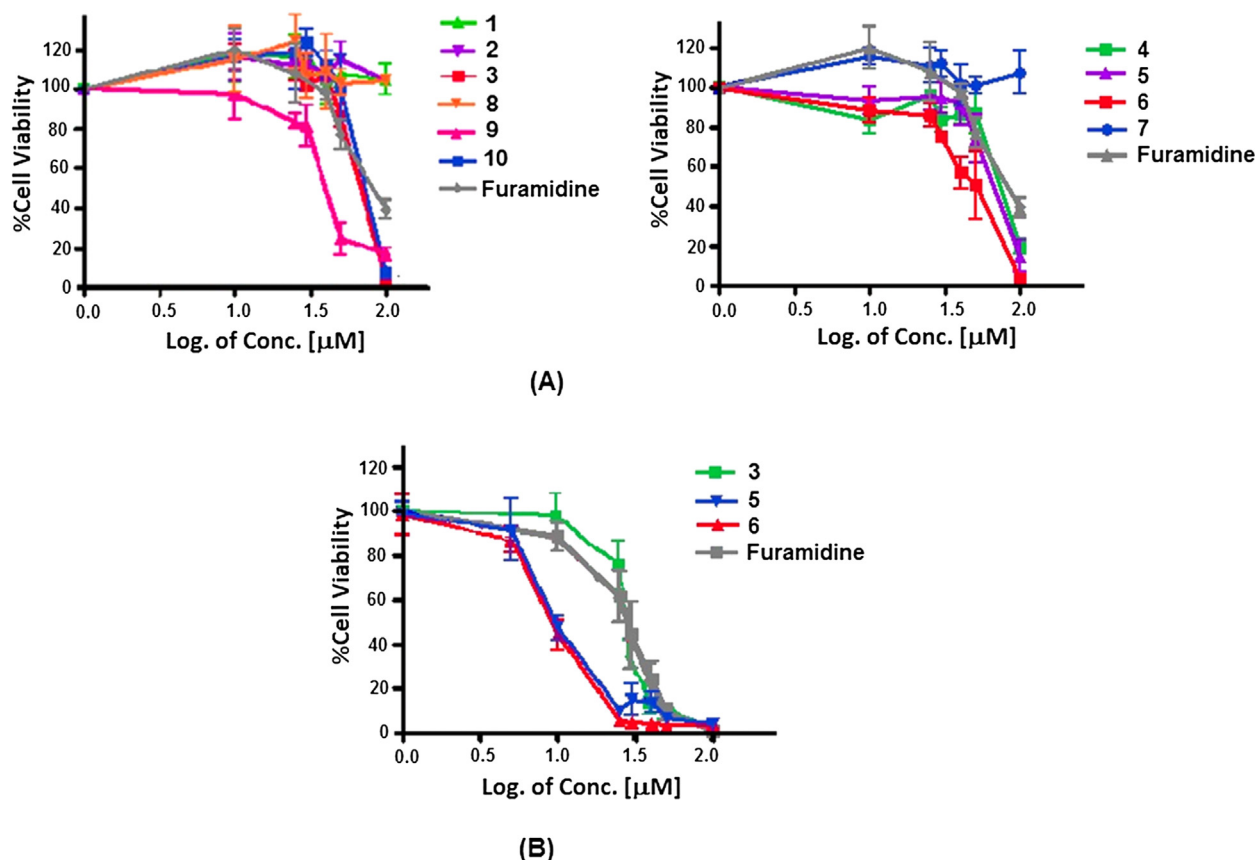


Fig. 6. The effects of (A) *bis*- and *mono*-isouronium (1–3 and 8–10) and *bis*-hydroxyguanidinium (4–7) derivatives on the viability of HL-60 and (B) *bis*-isouronium (3) and *bis*-hydroxyguanidinium (5–6) derivatives on the viability of Kelly cells as determined by AlamarBlue[®] assays. Cells were seeded at a density of 4×10^4 (HL-60) or 6×10^3 (Kelly) cells per well on a 96-well plate and treated with vehicle alone (1% (v/v) ddH₂O), or the compounds at 10–100 μM (HL-60) and 0.1–100 μM (Kelly). Furamidine was used as control. Cells were incubated for 72 h at 37 °C after which they were treated with AlamarBlue[®] and left in darkness in an incubator for 4.5 h. The resulting fluorescence was read using a plate reader from which percentage viability was calculated. The points on the graph represent mean values \pm S.E.M. from at least three independent experiments performed in triplicate.

In terms of *bis*- and *mono*-functionalised derivatives, four of the active compounds on the HL-60 cell line were di-cations; however, a *mono*-derivative (9) produced the lowest IC₅₀ value in the study. This result suggests that *mono*-derivatives may be inhibiting cell viability by alternative modes of action. A literature study of the uptake of furamidine and its analogues shows that those derivatives with two or four cations favour nuclear uptake whilst *mono*-cationic systems distribute into the cytoplasm and may enter the mitochondria [39,40]. Therefore, it is possible that the *mono*-functionalised agents in our study are acting similarly and may cause cell growth inhibition by an intrinsic apoptotic mechanism controlled by the mitochondria.

Considering that the different nature of the linker groups affects compound length and geometry, this feature may provide significant variation in compound activity. In our series, some of the most HL-60 active members possess the *-S-* linker irrespective of their cationic moieties (3, 6 and 10). Studies in the literature have shown that sulfur-containing compounds can induce apoptosis in HL-60 cells although the exact modes of action remain unclear [41]. In human cancer cells, a study of organosulfur compounds shows that they bind to tubulin and cause cell cycle arrest with the subsequent trigger of mitochondrial mediated apoptosis [42].

This general screening of growth inhibition in HL-60 cells provides evidence that, despite the poor binding to DNA, some of the isouronium and *N*-hydroxyguanidinium compounds induced significant inhibition and produced favourable IC₅₀ values, probably exerting their effects by alternative modes of action.

As in our previous study with *N*-hydroxyguanidines [9], we explored the cytotoxic potential of the best HL-60 cell growth inhibitors (IC₅₀ values <100 μM) in an additional cell line derived from a different cancer type. Thus, the cytotoxicity of isouronium derivatives 3, 9, 10 and 11 was evaluated in the Kelly (human neuroblastoma) cell line using the AlamarBlue[®] assay. Although a survey of the literature shows that the AlamarBlue[®] viability assay has seldom been used on Kelly cells, a recent study utilised this bioassay in the measure of cell proliferation and clonogenic growth [43]. Assays of each of the three derivatives were carried out in triplicate in at least three independent experiments. In these assays, the same concentration range was used as before, but once it was observed that the derivatives were having a substantial inhibitory effect on the Kelly cell line, additional lower concentrations (0.1–1 μM) were examined. Viability results and corresponding IC₅₀ values were obtained and are presented in Fig. 6B and Table 3.

All derivatives tested, except for the amide-linked compound 11, showed significant activity with IC₅₀ values between 17.3 and 33.9 μM (Table 2), comparing well with the IC₅₀ value obtained for furamidine (27.4 μM). Compared to our previous results with *N*-hydroxyguanidiniums, we observed that the overall potency obtained for both series of cationic systems is very encouraging, even more considering the resistant nature of neuroblastoma cells. Thus, the most potent derivatives were the *O*- and *S*-linked *bis*-hydroxyguanidiniums (5 and 6) which had IC₅₀ values of 11.7 ± 0.6 and 8.9 ± 1.0 μM , respectively. The isouronium derivatives exhibited

good IC₅₀ values of 17.3 ± 1.3 μM and 33.9 ± 1.2 μM for the *mono*-cationic **9** and **10** and 28.7 ± 1.76 μM for the *bis*-cationic **6** with compound **11** being the only inactive isouronium derivative (IC₅₀ > 100 μM) in this particular cell line.

Taking all this into consideration, activity in the Kelly cell line decreases from the *N*-hydroxyguanidinium derivatives to the isouroniums. Moreover, the *mono*-isouroniums **9** and **10** produced satisfactory IC₅₀ values in the same range as that of the *bis*-counterpart **6**. In addition, as with the previous cell line, it seems that DNA binding strength is irrelevant to the antiproliferative effect since compounds **10**, **5**, **6**, **9** and **10**, which are all poor DNA binders, produced satisfactory IC₅₀ values probably indicating a different mode of action. It is interesting that, the reference compound furamide, which is an excellent MGB, gave, in general, poorer cytotoxicity results than our compounds. In summary, our two cationic series were found to be encouraging tumour cell growth inhibitors, both in a representative diffuse (HL-60) and solid (Kelly) tumour cell lines, and thus, hold potential as anticancer agents.

2.5. Cell cycle and apoptosis studies

Having identified the effects of our compounds on cell viability both in HL-60 and Kelly cell lines, we next carried out flow cytometric analysis to discriminate between cell cycle arrest and/or induction of cell death. Thus, based on the IC₅₀ values obtained, *S*-linked isouronium derivatives **3** (*bis*-) and **10** (*mono*-) were assessed by flow cytometry on the HL-60 cell line (as described in the experimental section) and then compared to the results previously obtained for the *S*-linked *bis*-*N*-hydroxyguanidinium **6**.

Flow cytometry results are recorded as plots of peaks for each sample of treated and untreated cells with the horizontal axis representing increasing amounts of DNA and the vertical axis corresponding to cell number. In this case, 10,000 cells were monitored per experiment. Accordingly, each peak signifies cells consisting of a particular DNA content and, hence, is indicative of the proportion of cells in a particular phase of the cell cycle (Table 4). Apoptotic cells are subdiploid, given that characteristically programmed cell death is associated with nuclear fragmentation and as a result, a low (>2N) DNA content. The results from at least three independent experiments for the three compounds studied are presented in Table 4. Thus, at 24 h, it is evident that all the compounds have little effect on cell viability as indicated by the proportion of cells in the apoptotic (M1) peak (0.96 ± 0.25%–1.66 ± 0.55% in comparison to 0.81 ± 0.11% of the vehicle). Interestingly, **10** induces 9 ± 1.55%

apoptosis at 24 h. This was accompanied by an increase in the percentage of cells in the G₂/M (M4) phase (52.36 ± 5.21%) and in the polyploid G_n (M5) peak (11.58 ± 0.23%) in comparison to 16.73 ± 0.59% and 2.96 ± 0.79% of the vehicle-treated cells. As a result, there is a reduction in the number of cells in the synthesis phase (M3, S phase) and gap phase (M2, G₀/G₁ phase). This decrease is evident with only 11.17 ± 4.75% and 14.86 ± 2.8% in M2 and M3 compared to the vehicle 56.05 ± 1.4% and 24.46 ± 1.15%. This early effect suggests that compound **10** is toxic and elicits alternative cell cycle changes. The considerable increase of cells in the G₂/M phase (which indicates that cell cycle arrest is taking place) and increase in polyploid cells (G_n peak) suggests that this cell growth inhibitor may function not by inducing apoptosis but via an alternative mode of action.

At 48 h, analysis of M1 peaks shows that significant apoptosis has not been induced by the majority of the compounds. The *bis*-hydroxyguanidinium **6** shows modest apoptotic induction with 6.44 ± 1.55% cells in pre-G₁. Analysis of the phases M2 – M5 shows that the *bis*-isouronium **3** induces some G₂/M arrest (29.12 ± 10.73%) and polyploidy (8.42 ± 3.59%), but, in general, most values are analogous to those of the vehicle (Table 4). However, notable potency is observed with *mono*-isouronium **10** with more than 50% of the cells undergoing apoptosis and with evident reduction of the percentage of cells in M2, M3 and M4 phases. Considerable polyploidy (15.31 ± 7.53% to 3.02 ± 0.56% of the vehicle) has also been induced. Interestingly, comparison of the activity of **10** at 24 h suggests that the compound first induces cell cycle arrest which subsequently leads to apoptosis (Table 4).

The most significant changes are evident at the 72 h time-point. The most potent derivative was **10** with 39.89 ± 13.61% apoptosis. Interestingly, there is a slight increase in polyploidy (M5) cells (Table 4). Alternatively, as in the case of the *mono*-isouronium **10**, the *bis*-isouronium **3** has induced considerable cell cycle arrest at the G₂/M checkpoint (21.91 ± 6.34% in comparison to 10.53 ± 0.81% of the vehicle). In addition, a substantial population of cells has become polyploid with 22 ± 10.65% of cells in the G_n polyploidy peak in comparison to 3.43 ± 0.48% of the vehicle (Table 4).

From the results obtained by the flow cytometry experiments in the HL-60 cell line, it can be concluded that derivative **3** is a poor apoptotic-inducer at the chosen concentration (50 μM) and 24–72 h time-points, but alternative cell cycle events in the form of cell cycle arrest were observed. Thus, **3** shows an IC₅₀ of 57.4 ± 1.11 μM implying a stronger inhibitory effect at 50 μM than the resulting 4.87 ± 3.44% apoptotic cells. This may be justified

Table 4
Effects of the *bis*-isouronium **3** and the *mono*-isouronium **10** on the cycle of the HL-60 cells. Results for *bis*-hydroxyguanidinium **6** [18] are included for comparison. Cells were treated with 50 μM of compound and analysed by flow cytometry as described in the text and experimental section. Mean values ± S.E.M. of the proportion of cells of each phase of the cell cycle from at least three independent experiments are shown with M1 = pre-G₁ (<2N DNA), M2 = G₀/G₁ (2N DNA), M3 = S (2N – 4N DNA), M4 = G₂/M (4N DNA) and M5 = G_n (>4N DNA). Percentage apoptosis is determined from the M1 (pre-G₁) peak.

Compd. (50 μM)	M1 (pre-G ₁)	M2 (G ₀ /G ₁)	M3 (S)	M4 (G ₂ /M)	M5 (G _n)
24 h					
Vehicle	0.81 (±0.11)	56.05 (±1.4)	24.46 (±1.15)	16.73 (±0.59)	2.96 (±0.79)
3	1.46 (±0.38)	52.05 (±5.4)	26.92 (±2.87)	18.11 (±3.21)	3.11 (±0.66)
10	9.00 (±1.55)	11.17 (±4.75)	14.86 (±2.8)	52.36 (±5.21)	11.58 (±0.23)
6 [18]	1.53 (±0.28)	55.90 (±0.57)	25.85 (±2.23)	14.57 (±1.62)	2.35 (±0.98)
48 h					
Vehicle	1.41 (±0.32)	58.77 (±2.33)	24.29 (±1.37)	11.35 (±1.05)	3.02 (±0.56)
3	2.25 (±1.04)	38.27 (±12.59)	21.91 (±3.11)	29.12 (±10.73)	8.42 (±3.59)
10	55.50 (±18.73)	12.69 (±6.23)	10.42 (±4.46)	5.98 (±2.6)	15.31 (±7.53)
6 [18]	6.44 (±1.55)	56.62 (±6.66)	21.71 (±6.29)	10.78 (±0.39)	1.94 (±0.14)
72 h					
Vehicle	2.21 (±0.57)	59.50 (±1.50)	23.58 (±1.38)	10.53 (±0.81)	3.43 (±0.48)
3	4.87 (±3.44)	35.53 (±14.35)	15.59 (±3.39)	21.91 (±6.34)	22.00 (±10.65)
10	39.89 (±13.61)	18.21 (±6.26)	16.18 (±3.39)	8.67 (±2.14)	15.78 (±3.16)
6 [18]	22.20 (±6.97)	44.8 (±11.13)	15.99 (±4.7)	14.54 (±5.67)	2.10 (±0.33)

because the compound is highly potent with an average 95.8% inhibition of cell growth and proliferation at 100 μM and 30% cell inhibition at 50 μM as determined by viability studies. Having evaluated compound **3** in HL-60 cells by flow cytometry, it can be confirmed that its inhibitory power does not correspond to apoptosis but to cell cycle arrest at G_2/M and polyploidy (G_n). Therefore, **3** inhibits cell viability by causing cell cycle arrest. In comparison, **6** was found to induce considerable apoptotic activity with results of $22.2 \pm 6.97\%$ which correspond to an IC_{50} value of $46.4 \pm 1.08 \mu\text{M}$. More importantly, **10** was found to be the strongest apoptotic-inducer among the derivatives tested in the HL-60 cell line. As previously discussed, **10** was found to induce apoptosis at both 48 h and 72 h which corresponds to its IC_{50} value ($52.9 \pm 1.45 \mu\text{M}$) and also incite G_2/M arrest and polyploidy.

It is interesting to note that G_2/M arrest and polyploidy are associated with tubulin-targeting compounds [44–46]. Therefore, the ability of **10** to directly disrupt polymerisation of purified tubulin (the main component of the microtubular network) was studied *in vitro*. Inhibition of tubulin polymerisation was observed with compound **10** relative to the vehicle control (Fig. 7), indicating that this compound possesses tubulin depolymerising potential.

To further elucidate the apoptotic nature of compound **10** two key apoptotic events, which often occur following microtubular disruption, were also assessed: mitochondrial membrane depolarisation and caspase-3/7 activation. Treatment of HL-60 cells with compound **10** for 48 h resulted in statistically significant increases in both the percentage of cells displaying loss of mitochondrial membrane potential ($\Delta\Psi_m$, Fig. 8A) and caspase-3/7 activity (Fig. 8B) compared to vehicle-treated cells. Collectively, these results suggest that G_2/M arrest and subsequent apoptosis induced by compound **10**, are associated with microtubular depolymerisation, loss of mitochondrial membrane potential and activation of the caspase cascade in HL-60 cells.

Flow cytometry studies on the Kelly cell line were carried out on the O-linked *mono*-isouronium **9** which had an IC_{50} of $17.3 \pm 1.3 \mu\text{M}$. The experiments involved a modified procedure that had previously been employed for the suspension cells. The mean \pm S.E.M. values of at least three independent experiments for **9** at 25 μM and 50 μM are presented in Table 5. At 24 h compound **9** in the Kelly cell line induces some inhibitory activity with similar values obtained at both concentrations (Table 5). Therefore, in comparison to the

vehicle and control M1 peak values, compound **9** showed considerable cells in pre- G_1 . Correspondingly, no other significant phase activity such as cell cycle arrest was observed at this time-point. At 48 h, there is a further increase with ~50% of the total cells in M1 at 50 μM .

Evidently, compound **9** has a profound effect on the cell cycle with reductions by more than a half of cell numbers in the gap (M2 and M4) phases. Similar activity is observed at 25 μM with $38.02 \pm 5.71\%$ apoptosis. As before, no other additional cell cycle activity takes place. Finally, the activity observed is at its highest at 72 h for the two test concentrations ($48.35 \pm 3.5\%$ and $49.49 \pm 6.99\%$, respectively). As expected, the high proportion of cells undergoing apoptosis results in a drastic reduction of cell cycle activity and is most obvious in G_0/G_1 (M2) and G_2 (M4) stages. Taking the values presented in Table 5 into consideration, it is clear that **9** is cytotoxic towards the Kelly cell line and it is not surprising that it was found to be a strong apoptosis inducer by flow cytometry. Interestingly, no other cellular activities such as cell cycle arrest have taken place.

Based on these results, it is important to consider the structure-activity relationships of the O-linked *mono*-cationic isouronium (**9**), which despite exhibiting poor interactions with DNA, has been shown to induce encouraging cell cycle effects in the Kelly cell line. It may be possible that **9** targets an alternative organelle or pathway; thus, as mentioned, studies by Lansiaux et al. [36,37], show that furamidine *bis*-cationic derivatives (including the *bis*-guanidinium) readily accumulate in the nucleus while *mono*-cations distributed in the cytoplasm with possible mitochondrial accumulation. Despite this behaviour, a *mono*-cation in the same studies was found to be amongst the most cytotoxic agents. Therefore, a similar distribution pattern may be occurring here and overall, although **9** may target different upstream pathways, they both result in the same downstream effect of apoptotic cell death.

It is useful to compare the flow cytometry results of the HL-60 and Kelly cell lines. Firstly, in the HL-60 cells, **10** was found to be the strongest apoptosis inducer ($55.5 \pm 18.7\%$ at 50 μM) while in the Kelly cells, **9** was found to induce apoptosis at 25 μM ($48.35 \pm 3.50\%$). In the Kelly cell line, apoptosis is indicated by a gradual increase of the M1 population with a corresponding reduction of cells in remaining phases, whilst in HL-60 cells, cell cycle arrest and polyploidy are also observed. This is evident with

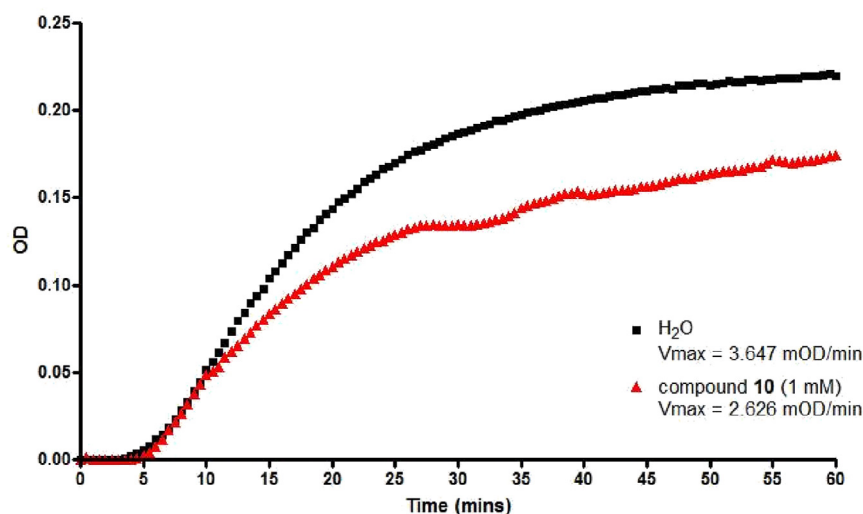


Fig. 7. Compound **10** reduced tubulin polymerisation *in vitro*. Purified bovine tubulin was incubated at 37 °C in the presence of either vehicle (1% (v/v) ddH₂O) or compound **10** (1 mM). Tubulin polymerisation was determined turbidimetrically at 340 nm at 30 s intervals for 60 min. The results represent the mean of three experiments. The V_{\max} values (mOD/min) refer to the rate of tubulin polymerisation over 60 min.

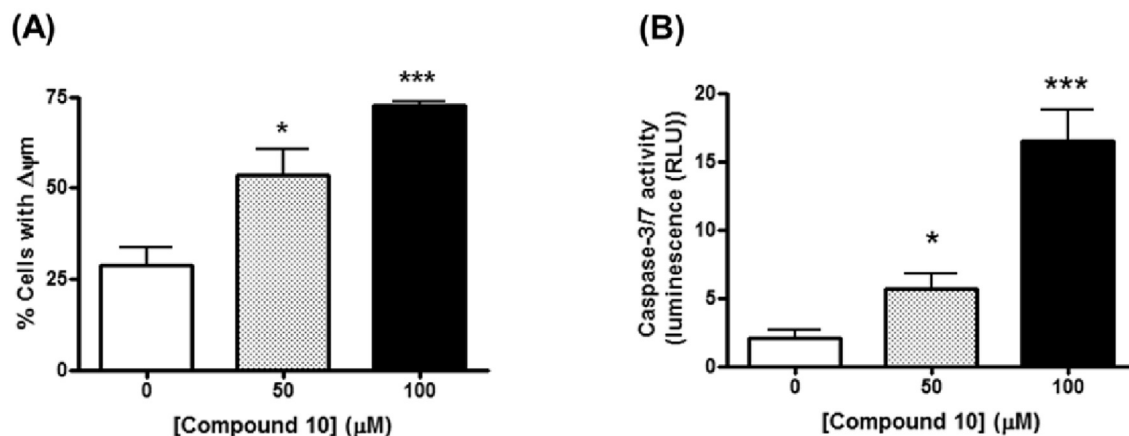


Fig. 8. Compound **10** induced mitochondrial depolarisation and caspase-3/7 activation in HL-60 cells. HL-60 cells ($200,000 \text{ cells mL}^{-1}$) were treated for 48 h with 0, 50 or 100 μM of compound **10**. (A) The cells were then stained with JC-1 for 30 min and their fluorescence (green and red) was determined by flow cytometry. An increase in green:red fluorescence was indicative of an increase in cytoplasmic JC-1 monomers and, thus, a loss of mitochondrial membrane potential ($\Delta\Psi\text{m}$). (B) Caspase-3/7 activity was determined using the Caspase-Glo Caspase-3/7 assay (Promega). The assay was performed according to the manufacturer's instructions and luminescence proportional to caspase activity was determined. Luminometer readings were normalised for cell viability which was determined by AlamarBlue[®] assay. For both assays, values shown represent the mean \pm SEM for at least three independent experiments. A P -value of less than 0.05 was considered to be statistically significant (* $P < 0.05$, *** $P < 0.001$).

10 which induced more than 50% cell cycle arrest followed by apoptosis. Therefore, it can be confirmed that the derivatives in this study induce different cell cycle effects. It may be possible that different upstream pathways are being targeted but that simultaneously downstream apoptotic effects are being observed. Further studies would have to be carried out in order to confirm their exact mode of action.

2.6. Studies in non-cancerous cells

Since we have established that select isouronium derivatives can inhibit cell growth and induce apoptosis in cancer cells, their toxicity in non-tumourigenic cell lines such as NIH/3T3 (murine fibroblast cell line) and MCF-10A (human breast epithelial cell line) was next investigated. Both of these cell lines were treated with 50 or 100 μM solutions of compound **10** for 72 h and then cell viability was assessed by the AlamarBlue[®] assay and percentage apoptosis evaluated by flow cytometry as described above for cancer cells. It was found that treatment with compound **10** led to no loss of cell viability in MCF-10A cells and only minimal loss in NIH/3T3 at concentrations that were highly toxic to cancer cells (Fig. 9A). In

contrast to the significant levels of apoptosis ($63.6\% \pm 7.2$ with 100 μM) induced by compound **10** in HL-60 cells, this derivative did not induce increased levels of apoptosis in the non-cancerous NIH/3T3 or MCF-10A cells (Fig. 9B). This finding illustrated that the small reduction in viability observed in NIH/3T3 cells could be attributed to cell cycle arrest rather than to apoptosis.

3. Conclusions

The suitability of the isouronium and *N*-hydroxyguanidinium cations as HB donors/acceptors has been compared in terms of computational DFT studies. Considering the good binding expected by these groups, the ability of a family of *bis*- and *mono*-isouronium compounds to bind to DNA has been measured by means of DNA thermal denaturation experiments and compared to the results previously obtained with a family of *bis-N*-hydroxyguanidines. As a result of the poor DNA binding observed, the nature of the diamromatic linker has been explored and thus the corresponding amide-linked *bis*-isouronium derivative has been synthesised and its DNA affinity measured by thermal melting experiments. From these studies it can be concluded that for optimal DNA binding two

Table 5
The effects of the *mono*-isouronium **9** on the cell cycle of the Kelly cell line. Cells were treated with 25 μM and 50 μM and analysed by flow cytometry as described in the text and experimental section. Mean values \pm S.E.M. of the proportion of cells of each phase of the cell cycle from at least three independent experiments are shown with **M1** = pre-G₁ (<2N DNA), **M2** = G₀/G₁ (2N DNA), **M3** = S (2N – 4N DNA), **M4** = G₂/M (4N DNA) and **M5** = G_n (>4N DNA). Percentage apoptosis is determined from the **M1** (pre-G₁) peak.

Compd	M1 (pre-G ₁)	M2 (G ₀ /G ₁)	M3 (S)	M4 (G ₂)	M5 (G _n)
24 h					
Control	5.84 (± 1.92)	52 (± 2.21)	19.02 (± 1.24)	13.83 (± 1.22)	8.81 (± 1.79)
Vehicle	6.12 (± 0.95)	52.37 (± 1.44)	18.67 (± 1.90)	13.12 (± 0.93)	9.85 (± 1.54)
9 (25 μM)	20.41 (± 3.99)	31.2 (± 3.23)	25.59 (± 2.40)	11.27 (± 0.45)	13.49 (± 1.06)
9 (50 μM)	24.33 (± 6.65)	42.14 (± 2.39)	15.98 (± 2.21)	8.23 (± 1.40)	7.77 (± 0.81)
48 h					
Control	5.43 (± 2.11)	50.74 (± 1.72)	18.89 (± 0.67)	14.16 (± 0.49)	8.55 (± 0.41)
Vehicle	5.88 (± 1.13)	52.54 (± 2.32)	19.05 (± 2.11)	13.68 (± 0.74)	8.97 (± 1.27)
9 (25 μM)	38.02 (± 5.71)	22.2 (± 1.06)	27.52 (± 2.71)	7.65 (± 1.38)	6.91 (± 0.62)
9 (50 μM)	50.72 (± 5.65)	25.17 (± 1.04)	11.71 (± 0.45)	3.5 (± 0.49)	4.19 (± 0.06)
72 h					
Control	8.1 (± 1.48)	51.78 (± 3.36)	16.84 (± 0.55)	13.45 (± 0.57)	10.21 (± 1.87)
Vehicle	10.21 (± 2.85)	46.82 (± 1.46)	16.29 (± 0.81)	13.84 (± 0.76)	13.07 (± 0.25)
9 (25 μM)	48.35 (± 3.50)	26.17 (± 2.64)	16.38 (± 4.82)	5.04 (± 0.88)	4.09 (± 0.64)
9 (50 μM)	49.49 (± 6.99)	29.01 (± 5.64)	17.34 (± 3.52)	2.44 (± 0.28)	2.69 (± 0.26)

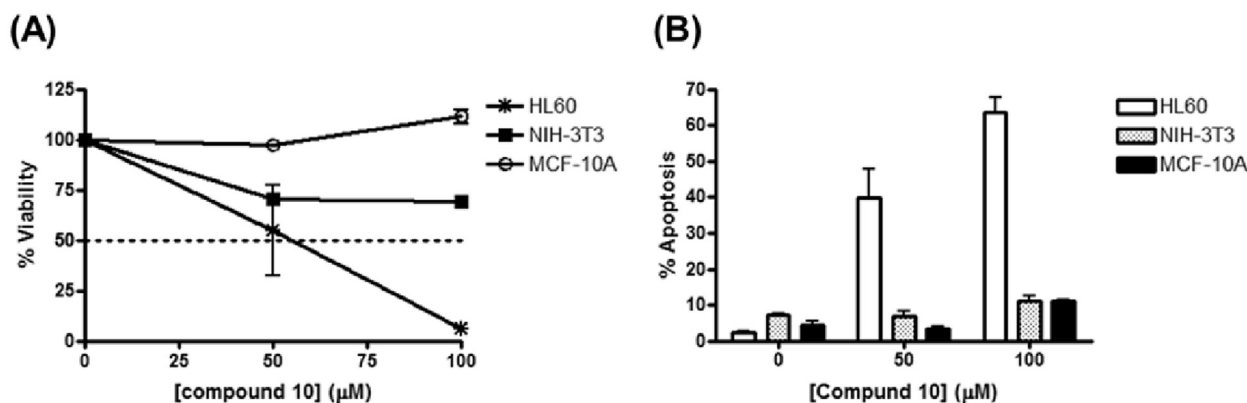


Fig. 9. Compound **10** induced apoptosis in HL-60 leukemia cells with minimal toxicity to non-cancerous NIH3T3 and MCF-10A cell lines. HL-60, NIH-3T3 and MCF-10A cells were treated with 0 (vehicle, 1% (v/v) dH₂O), 50 or 100 μM compound **10** for 72 h. (A) Cell viability was assessed by detecting the reduction of AlamarBlue™ (10% (v/v)) using a fluorimeter. (B) Apoptosis was measured by fixing the cells in ice-cold 70% (v/v) EtOH/PBS and staining their DNA with propidium iodide. Propidium iodide fluorescence was proportional to the quantity of DNA in each entity. Cells with sub-diploid DNA contents were deemed apoptotic. Results represent the mean ± S.E.M for at least 3 experiments.

cations need to be present in this type of diatomic systems and that the presence of a HB acceptor in these cations is detrimental for the DNA binding.

The inhibitory effects of *mono*- and *bis*-isouronium series of compounds were evaluated on two different cancer cell lines and compared with the previously reported *bis-N*-hydroxyguanidinium. Accordingly, IC₅₀ values were found to be 36.9–57.4 μM (HL-60), and 17.3–33.9 μM (Kelly), and are comparable to the IC₅₀ values previously found for the *N*-hydroxyguanidine series. Compounds with the *-S-* linker (**3**, **6**, and **10**) proved to be considerably active in the HL-60 cells and even more active in the Kelly cell lines. In general, regarding the nature of the cation, the activity decreases from the *N*-hydroxyguanidiniums to the isouroniums.

No correlation was found between DNA minor groove binding and cell growth inhibition; hence, activity may depend on different modes of action. The *mono*-derivatives may not enter the nucleus and may function in the extranuclear cytoplasm by targeting an alternative target (such as the mitochondria or microtubules) or pathway. In fact, results obtained with HL-60 cells suggest that G₂/M arrested and subsequent apoptosis induced by compound **10** are associated with microtubular depolymerisation, loss of mitochondrial membrane potential and activation of the caspase cascade.

Considering the results from the viability assays and flow cytometry studies, it can be concluded that besides inhibiting cell viability and proliferation, derivatives **9** and **10** are significant apoptosis-inducers in the HL-60 and Kelly cell lines. Moreover, the effects of compound **10** on cell viability and apoptosis in two non-cancerous cell lines (NIH3T3 and MCF-10A) compared to HL-60 cells, indicate no toxic effects (MCF-10A) or minimal toxicity (NIH/3T3). In particular, special attention should be paid to the high potency and low IC₅₀ values observed in the resistant neuroblastoma Kelly cell line. Taking into consideration the need for novel therapies for this type of cancer, these are very encouraging results making these derivatives excellent candidates for potential cancer therapeutic agents.

4. Experimental

4.1. Computational methods

Complexes between phenylguanidinium, *O*-phenylisouronium, and phenyl-*N*-hydroxyguanidinium with HF and HCOH in different orientations were optimised using the Gaussian09 package [47] at

the M06-2X and MP2 computational levels with the 6-311++G** basis set. Frequency calculations were performed at the same computational level to confirm that the resulting optimised structures are energetic minima.

Effects of water solvation have been included by means of the SCFR-PCM approaches implemented in the Gaussian09 package including dispersing, repulsing, and cavitating energy terms of the solvent starting from the gas-phase geometries and re-optimising. The electron density of the complexes has been analysed within the Atoms in Molecules (AIM) theory.

4.2. Chemistry

All commercial chemicals were obtained from Sigma–Aldrich or Fluka and were used without further purification. Deuterated solvents for NMR use were purchased from Apollo. Dry solvents were prepared using standard procedures, according to Vogel, with distillation prior to use. Chromatographic columns were run using Silica gel 60 (230–400 mesh ASTM). Solvents for synthetic purposes were used at GPR grade. Analytical TLC was performed using Merck Kieselgel 60 F₂₅₄ silica gel plates. Visualisation was by UV light (254 nm). NMR spectra were recorded in a Bruker DPX-400 Avance spectrometer, operating at 400.13 MHz and 600.1 MHz for ¹H NMR and 100.6 MHz and 150.9 MHz for ¹³C NMR. Shifts are referenced to the internal solvent signals. NMR data were processed using Bruker Win-NMR 5.0 software. Electrospray mass spectra were recorded on a Mass Lynx NT V 3.4 on a Waters 600 controller connected to a 996 photodiode array detector with methanol as carrier solvent. Melting points were determined using an Electrothermal IA9000 digital melting point apparatus and are uncorrected. Elemental analysis was carried out at the Microanalysis Laboratory, School of Chemistry and Chemical Biology, University College Dublin. Analyses indicated by the symbols of the elements or functions were within ±0.4% of the theoretical values. Furamide was kindly donated to our group by Prof. D.W Wilson (Georgia State University, USA).

4.2.1. 4-Hydroxy-*N*-(4-hydroxyphenyl)benzamide (**12**)

A solution of 4-hydroxybenzoic acid (0.276 g, 2 mmol) in SOCl₂ (4 mL) and anhydrous DMF (5 drops) was refluxed for 3.5 h, after which excess SOCl₂ was removed by distillation and under vacuum giving an off-white solid. The amine solution was prepared by dissolving 4-aminophenol (0.655 g, 6 mmol) in dry DMF (4 mL) along with a catalytic amount of DMAP (0.012 g, 0.1 mmol, 5%) and

was kept at 0 °C under argon. The acid chloride was then dissolved in dry DMF (10 mL) and added drop-wise *via* syringe to the amine under argon. The solution was stirred overnight at 0 °C under argon. Then the solution was dissolved in EtOAc after which a precipitate crashed out. This was removed by suction filtration and the organic layer washed with 2M HCl solution (6 × 30 mL), saturated NaHCO₃ (60 mL) and brine (60 mL). It was dried with anhydrous Na₂SO₄ and concentrated under vacuum. Yellow solid (63%); mp, decomposes over 250 °C (lit. 268–269 °C [48]); IR (ATR) 3623, 3383, 1644, 1538, 1506, 1435, 1378, 1335, 1323, 1242, 1168, 1119, 1103, 1074, 1045, 971, 958, 933, 903, 827, 777, 762, 660, 643, 632, 615, 605 cm⁻¹; ¹H NMR (400 MHz, DMSO-*d*₆) δ 6.72 (d, 2H, *J* = 8.0 Hz, Ar.), 6.84 (d, 2H, *J* = 8.0 Hz, Ar.), 7.5 (d, 2H, *J* = 8.0 Hz, Ar.), 7.82 (d, 2H, *J* = 8.0 Hz, Ar.), 9.76 (br s, 1H); ¹³C NMR (400 MHz, DMSO-*d*₆) δ 114.8, 114.9, 122.2, 125.5129.5, 131, 153.4, 160.4 (Ar.), 164.6 (CO); HRMS (*m/z* -ES) 228.0661 calcd [M⁺-H]; found 228.0658.

4.2.2. 4-[*N,N'*-Di(*tert*-butoxycarbonyl)carbamimidoyloxy]-*N*-{4-[*N,N'*-di(*tert*-butoxy carbonyl)carbamimidoyloxy]phenyl}benzamide (**14**)

To a solution of 85 mg (0.37 mmol) of **12** and 205 mg (0.74 mmol) of Boc-protected *S*-methylisothiourea, HgCl₂ (0.81 mmol, 221 mg) and 0.4 mL (3.6 mmol) of TEA in dry DMF (1 mL) were added at 0 °C. The mixture was stirred for 1.5 h at 0 °C and a further 24 h at rt. Then, it was dissolved in EtOAc, the HgS precipitate filtered through a pad of celite and the organic layer washed with water (2 × 30 mL) and brine (30 mL), dried over anhydrous Na₂SO₄ and concentrated under vacuum. Purification by silica gel chromatography using hexane:EtOAc (3:2) afforded **14** as a white solid (58 mg) (22%). In an alternative synthesis, HgCl₂ (1.85 mmol, 502 mg) was added over 191 mg (0.84 mmol) of **12** and 488 mg (1.68 mmol) of Boc-protected thiourea and 0.9 mL (8.1 mmol) of TEA in dry DMF (3 mL) at 0 °C. The resulting mixture was treated as above and the product purified by silica gel chromatography using hexane:EtOAc (2:1) afforded **14** as a white solid (1749 mg) (29%); mp, 141–143 °C; IR (ATR) 3280, 1770, 1660, 1625 cm⁻¹; ¹H NMR (400 MHz, DMSO-*d*₆) δ 1.35 (s, 18H, (CH₃)₃), 1.45 (s, 18H, (CH₃)₃), 7.11 (d, 2H, *J* = 9.0 Hz, Ar.), 7.29 (d, 2H, *J* = 8.5 Hz, Ar.), 7.79 (d, 2H, *J* = 9.0 Hz, Ar.), 7.99 (d, 2H, *J* = 8.5 Hz, Ar.), 10.4 (br s, 1H), 10.83 (br s, 1H), 10.95 (br s, 1H); ¹³C NMR (400 MHz, CDCl₃-*d*₆) δ 28.2 (2(CH₃)₃), 31.2 (2(CH₃)₃), 81.9, (2C(CH₃)₃), 82.1 (2C(CH₃)₃), 121.8, 122.5, 129.8, 133.0, 137.3, 147.3, 150.6, 151.5 (Ar.), 151.5 (CO), 152.1 (CO), 157.7 (CN), 158 (CN) 165.3 (CO); HRMS (*m/z* -ES) 736.3170 calcd [M⁺ + Na]; found 736.3164.

4.2.3. 4-(Carbamimidoyloxy)-*N*-[4-(carbamimidoyloxy)phenyl]benzamide dihydrochloride salt (**11**)

In excess (8 mL) TFA/DCM (50:50), compound **14** (0.24 mmol, 171 mg) was dissolved and stirred at rt for 3 h. The solvent was then eliminated under vacuum to generate the trifluoroacetate salt as a colourless oil. This was dissolved in H₂O (5 mL) and treated for 12.5 h with IRA400 Amberlite resin in its Cl⁻ form. The resin was then removed by filtration and the aqueous solution washed with DCM (3 × 30 mL). Evaporation of the water, followed by purification by reverse-phase chromatography afforded the hydrochloride salt. Absence of the trifluoroacetate salt was checked by ¹⁹F NMR. The product was an off-white solid (80 mg) (86%); mp, decomposes over 162 °C; IR (ATR) 3579, 3545, 1671, 1650, 1537, 1489, 1446, 1406, 1322, 1313, 1301, 1267, 1205, 1175, 1166, 1098, 1014, 980, 905, 875, 845, 792, 765, 728, 637, 624, 611, 604 cm⁻¹; ¹H NMR (400 MHz, D₂O) δ 7.28 (d, 2H, *J* = 8.0 Hz, Ar.) 7.39 (d, 2H, *J* = 7.5 Hz, Ar.), 7.59 (d, 2H, *J* = 8.0 Hz, Ar.), 7.91 (d, 2H, *J* = 7.5 Hz, Ar.); ¹³C NMR (400 MHz, D₂O) δ 121.2, 121.5, 123.9, 129.8, 133.2, 136.2, 145.8, 151.4 (Ar.), 160.9 (CN), 161.3 (CN), 167.8 (CO); HRMS (*m/z* -ES) 314.1253 calcd

[M⁺ + H]; found 314.1259. Anal. C₁₅H₁₇Cl₂N₅O₃ (C, H, N, O).

4.3. Biophysical experiments

4.3.1. DNA thermal denaturation assays with DNA salmon sperm DNA

Thermal melting experiments were conducted with a Varian Cary 300 Bio spectrophotometer equipped with a 6 × 6 multicell temperature-controlled block. Temperature was monitored with a thermistor inserted into a 1 mL quartz cuvet containing the same volume of water as in the sample cells. Absorbance changes at 260 nm were monitored from a range of 20 °C–90 °C with a heating rate of 1 °C min⁻¹ and a data collection rate of five points per °C. The salmon sperm DNA was purchased from Sigma Aldrich (extinction coefficient ε₂₆₀ = 6600 cm⁻¹ M⁻¹ base). A quartz cell with a 1-cm path length was filled with a 1 mL solution of DNA polymer or DNA-compound complex. The DNA polymer (150 μM base) and the compound solution (15 μM) were prepared in a phosphate buffer (0.01 M Na₂HPO₄/NaH₂PO₄), adjusted to pH 7 so that a compound to DNA base ratio of 0.1 was obtained. The thermal melting temperatures of the duplex or duplex-compound complex obtained from the first derivative of the melting curves are reported.

4.4. Biochemistry

4.4.1. Cell culture

Human promyelocytic leukemia HL-60 cells, mouse embryonic fibroblast NIH/3T3 cells and human breast epithelial MCF-10A cells were originally obtained from the ATCC (Manassas, VA, USA) while human neuroblastoma Kelly cells were originally obtained from the ECACC (Salisbury, UK). All cells were cultured in a humidified incubator at 37 °C in 5% CO₂. HL-60 and Kelly cells were cultured in RPMI-1640 with GlutaMax I and supplemented with 10% foetal bovine serum, 50 U mL⁻¹ penicillin and 50 μg mL⁻¹ streptomycin while NIH/3T3 cells were maintained in Dulbecco's Modified Eagle Medium (DMEM) with GlutaMax I supplemented with 10% (v/v) foetal bovine serum and 10 μg mL⁻¹ ciprofloxacin and MCF-10A cells were grown in Dulbecco's Modified Eagle Medium: Nutrient Mixture F-12 (DMEM/F12) supplemented with 5% (v/v) horse serum, 20 ng mL⁻¹ epidermal growth factor, 0.5 μg mL⁻¹ hydrocortisone, 100 ng mL⁻¹ cholera toxin, 10 μg mL⁻¹ insulin, and 1% (v/v) penicillin/streptomycin. HL-60 cells were maintained at a density between 200,000 and 1,000,000 cells mL⁻¹ and adherent cells were subcultivated by trypsinisation prior to reaching confluency.

4.4.2. Treatment of the cells with the compounds studied

The dried compounds were re-suspended in sterile ddH₂O to yield 10 mM stock solutions. The solutions were sterile filtered and required concentration ranges (10–0.1 mM) of each drug were prepared in sterile ddH₂O and stored at –20 °C until required. HL-60 cells were seeded at 200,000 cells mL⁻¹ in complete medium and treated with a range of concentrations of the compounds to yield final concentrations between 1 and 100 μM. Kelly cells seeded at 30,000 cells mL⁻¹ were treated with a range of concentrations of the compounds to yield final concentrations in the cells between 0.01 and 100 μM. NIH/3T3 and MCF-10A cells were seeded at 6000 cells per cm² and treated to yield final concentrations of either 50 or 100 μM compound **10**.

4.4.3. Cell viability (AlamarBlue®)

HL-60 cells in the log phase of growth were seeded in 96-well plates at a density of 200,000 cells mL⁻¹ (200 μL/well or 40,000 cells/well). Adherent Kelly cells were seeded at 30,000 cells mL⁻¹ (200 μL/well or 6000/well), NIH/3T3 and MCF-

10A were seeded at 10,000 cells mL⁻¹ (200 μL/well or 2000/well) and incubated at 37 °C for 24 h prior to treating. All the cells were then treated with a 1:100 dilution of stock concentrations of drugs or ddH₂O as vehicle control in triplicate. Three blank wells containing 200 μL media with no cells plus 20 μL AlamarBlue[®] were also set up as blanks. After 72 h incubation, 20 μL AlamarBlue[®] was added to each well. The plates were incubated in darkness at 37 °C for 4.5 h. Using a Molecular Devices microplate reader, the fluorescence (F) was then read at an excitation wavelength of 544 nm and an emission wavelength of 590 nm. Cell viability was then determined by subtracting the mean blank fluorescence (F_b) from the treated sample fluorescence (F_s) and expressing this as a percentage of the fluorescence of the vehicle control (F_c). The results were then plotted as nonlinear regression, sigmoidal dose–response curves on Prism, from which the IC₅₀ value for each drug was determined.

4.4.4. Determination of DNA content (Flow cytometry)

HL-60 cells were seeded at 200,000 cells mL⁻¹ in T25 flasks and treated with appropriate drug concentrations and ddH₂O as vehicle control for 24 h, 48 h and 72 h time-points. Cells were harvested at each time-point by centrifugation at 300× g for 8 min. Kelly cells were seeded at 120,000 cells mL⁻¹ on six-well plates and left to incubate at 37 °C for 24 h. NIH/3T3 and MCF-10A were seeded at 6000 cell per cm² on 12-well plates and similarly incubated for 24 h. The cells were then treated with compound and harvested at the required times. Adherent cells were washed with PBS, trypsinised and collected by centrifugation at 300× g for 8 min. In both types of cells, media was drained and the pellets resuspended in 200 μL non-sterile PBS. The cells were then fixed by a drop-wise addition of 2 mL of ice-cold 70% EtOH/PBS while vortexing. Following overnight fixation at –20 °C, 10 μL of FBS was added to the cells and the solutions centrifuged at 2200 RPM for 10 min. The ethanol was then drained and the cell pellet resuspended in 0.4 mL PBS. RNase A (25 μL 10 mg mL⁻¹), which destroys RNA so that only DNA can be observed, was then added. Propidium iodide (PI, 75 μL, 1 mg mL⁻¹), a DNA binding dye which fluoresces when activated and thus allows the amount of DNA present to be determined, was also added to each sample. Cells were vortexed and incubated in the dark at 37 °C for 30 min. The PI fluorescence was measured on a linear scale using a FACS Calibur flow cytometer (HL-60 and Kelly) or BD Accuri C6 (NIH/3T3 and MCF-10A) both from Becton Dickinson, San Jose, CA. Data collections (10,000 events per sample) were gated to exclude cell debris and cell aggregates. The amount of fluorescence is proportional to the amount of DNA present and hence the population of cells in each phase of the cell cycle can be determined. Cells are gated as follows: M1 = pre-G₁ (<2N DNA), M2 = G₀/G₁ (2N DNA), M3 = S (2N – 4N DNA), M4 = G₂/M (4N DNA), M5 = (G_n > 4N DNA). Apoptotic cells are hypoploid (<2N DNA). Therefore, apoptosis was determined from the peak in M1. All data was recorded and analysed using the CellQuest or Accuri C6 software (Becton Dickinson, San Jose, CA).

4.4.5. Tubulin polymerisation assay

The assembly of purified bovine tubulin was monitored using a kit, BK006, purchased from Cytoskeleton Inc., (Denver, CO, USA). The assay was carried out in accordance with the manufacturer's instructions using the standard assay conditions. Briefly, purified (>99%) bovine brain tubulin (3 mg/ml) in a buffer consisting of 80 mM PIPES (pH 6.9), 0.5 mM EGTA, 2 mM MgCl₂, 1 mM GTP and 10% glycerol was incubated at 37 °C in the presence of either vehicle (1% (v/v) ddH₂O) or compound 13 (1 mM). Light is scattered proportionally to the concentration of polymerised microtubules in the assay. Therefore, tubulin assembly was monitored turbidimetrically at 340 nm in a Spectramax

340 PC spectrophotometer (Molecular Devices, Sunnyvale, CA, USA). The absorbance was measured at 30 s intervals for 60 min.

4.4.6. Loss of mitochondrial membrane potential ($\Delta\Psi_m$)

Mitochondrial transmembrane potential was measured using the potentiometric dye 5,5',6,6'-tetrachloro-1,1',3,3'-tetraethylbenzimidazolyl-carbocyanine iodide (JC-1) (Molecular Probes, Invitrogen, Germany). In healthy cells, JC-1 accumulates in the mitochondria where it spontaneously forms aggregates which fluoresce red. In cells with low mitochondrial membrane potential JC-1 remains in cytoplasm in monomers which fluoresce green. Following treatment, the cells were washed with PBS and stained with JC-1 (5 μM) in PBS for 30 min at 37 °C. Cells were washed with PBS, resuspended in ice-cooled PBS and immediately assessed for green and red fluorescence by flow cytometry (BD Accuri C6, Becton Dickinson, San Jose, CA). Excitation at 488 nm and emission filters of 535 and 595 nm were used to quantify the population of mitochondria with green (JC-1 monomers) and red (JC-1 aggregates) fluorescence, respectively. An increase in the ratio of green:red fluorescence indicated loss of mitochondrial membrane potential ($\Delta\Psi_m$). The percentage of cells displaying $\Delta\Psi_m$ was calculated using Flowjo software (Tree Star Inc., Oregon, USA).

4.4.7. Caspase-3/7 activity assay

HL-60 cells were seeded onto 96-well plates (20,000 cells/100 μL) and treated for 48 h. Cell viability was then measured using AlamarBlue[™] as described above. Caspase-3/7 activity was then measured using the Caspase-Glo[®] caspase-3/7 luminescent assay in accordance with the manufacturer's instructions (Promega, Madison, WI, USA). Briefly, the cells were lysed by addition of an equal volume of Caspase-Glo[®] reagent and incubation on an orbital plate shaker for 1 h at room temperature in darkness. The reagent also contained a luminogenic substrate containing the DEVD sequence specific for caspases-3 and -7. Once cleaved this substrate released aminoluciferin which subsequently reacted with luciferase resulting in the production of light which was then quantified using a luminometer. Readings were normalised for cell viability.

Acknowledgments

This research was supported by Science Foundation Ireland (SFI–RFP: CHE275). A.K.S. thanks SFI for generous funding. The authors thank Dr. C. Trujillo for her assistance with the computational study.

Appendix A. Supplementary data

Supplementary data related to this article can be found at <http://dx.doi.org/10.1016/j.ejmech.2016.03.047>.

References

- [1] M.P. Barrett, C.G. Gemmill, C.J. Suckling, Minor groove binders as anti-infective agents, *Pharmacol. Ther.* 139 (2013) 12–23.
- [2] R.K. Arafa, M.A. Ismail, M. Munde, W.D. Wilson, T. Wenzler, R. Brun, D.W. Boykin, Novel linear triaryl guanidines, N-substituted guanidines and potential prodrugs as antiprotozoal agents, *Eur. J. Med. Chem.* 43 (2008) 2901–2908.
- [3] P.B. Dervan, Molecular recognition of DNA by small molecules, *Bioorg. Med. Chem.* 9 (2001) 2215–2235.
- [4] S. Lang, A.I. Khalaf, D. Breen, J.K. Huggan, C.J. Clements, S.P. MacKay, C.J. Suckling, Oligoamides of 2-amino-5-alkylthiazole 4-carboxylic acids: anti-trypanosomal compounds, *Med. Chem. Res.* 23 (2014) 1170–1179.
- [5] X. Zhang, S.C. Zhang, D. Sun, J. Hu, A. Wali, H. Pass, F. Fernandez-Madrid, M.R. Harbut, N. Tang, New insight into the molecular mechanisms of the biological effects of DNA minor groove binders, *PLoS One* 6 (2011) e25822.
- [6] M.F. Paine, M.Z. Wang, C.N. Generaux, D.W. Boykin, W.D. Wilson, H.P. De Koning, C.A. Olson, G. Pohlrig, C. Burri, R. Brun, G.A. Murilla, J.K. Thuita, M.P. Barrett, R.R. Tidwell, Diamidines for human African trypanosomiasis,

- Curr. Opin. Investig. Drugs 11 (2010) 876–883.
- [7] M. Sands, M.A. Kron, R.B. Brown, Pentamidine: a review, *Rev. Infect. Dis.* 7 (1985) 625–634.
- [8] W. Mulugeta, J. Wilkes, W. Muluat, P.A.O. Majiwa, R. Masake, A.S. Peregrine, Long-term occurrence of Trypanosoma congolense resistant to diminazene, isometamidium and homidium in cattle at Ghibe, Ethiopia, *Acta Trop.* 64 (1997) 205–217.
- [9] F. Yang, N.G. Nickols, B.C. Li, G.K. Marinov, J.W. Said, P.B. Dervan, Antitumor activity of a pyrrole-imidazole polyamide, *Proc. Natl. Acad. Sci. U. S. A.* 110 (2013) 1863–1868.
- [10] N.G. Anthony, D. Breen, G. Donoghue, A.I. Khalaf, S.P. Mackay, J.A. Parkinson, C.J. Suckling, A new synthesis of alkene-containing minor-groove binders and essential hydrogen bonding in binding to DNA and in antibacterial activity, *Org. Biomol. Chem.* 7 (2009) 1843–1850.
- [11] G. He, E. Vasilieva, G.D. Harris Jr., K.J. Koeller, J.K. Baskin, C.M. Dupureur, Binding studies of a large antiviral polyamide to a natural HPV sequence, *Biochimie* 102 (2014) 83–91.
- [12] F. Rodriguez, I. Rozas, M. Kaiser, R. Brun, B. Nguyen, W.D. Wilson, R.N. Garcia, C. Dardonville, New bis(2-aminoimidazoline) and bisguanidine DNA minor groove binders with potent in vivo antitrypanosomal and antiplasmodial activity, *J. Med. Chem.* 51 (2008) 909–923.
- [13] P.S. Nagle, F. Rodriguez, A. Kahvedžić, S. Quinn, I. Rozas, Asymmetrical Di-aromatic guanidinium/2-aminoimidazolium derivatives: synthesis and DNA affinity, *J. Med. Chem.* 52 (2009) 7113–7121.
- [14] P.S. Nagle, F. Rodriguez, S.J. Quinn, D.H. O'Donovan, J.M. Kelly, B. Nguyen, W.D. Wilson, I. Rozas, Understanding the DNA binding of novel non-symmetrical guanidinium/2-aminoimidazolium derivatives, *Org. Biomol. Chem.* 8 (2010) 5558–5567.
- [15] P.S. Nagle, F. Rodriguez, B. Nguyen, W.D. Wilson, I. Rozas, High DNA affinity of a series of amide linked aromatic dicationic, *J. Med. Chem.* 55 (2012) 4397–4406.
- [16] P. O'Sullivan, I. Rozas, Understanding the guanidine-like cationic moiety for optimal binding into the DNA minor groove, *Chem. Med. Chem.* 9 (2014) 2063–2073.
- [17] P.S. Nagle, C. McKeever, F. Rodriguez, B. Nguyen, W.D. Wilson, I. Rozas, Unexpected DNA affinity and sequence selectivity through core rigidity in guanidinium-based minor groove binders, *J. Med. Chem.* 55 (2014) 4397–4406.
- [18] A. Kahvedžić, S.M. Nathwani, D.M. Zisterer, I. Rozas, Aromatic bis-hydroxyguanidinium derivatives: synthesis, biophysical and biochemical evaluations, *J. Med. Chem.* 56 (2013) 451–459.
- [19] A. Goonan, A. Kahvedžić, F. Rodríguez, P.S. Nagle, T. McCabe, I. Rozas, A.M. Erdozain, J.J. Meana, L.F. Callado, Novel synthesis and pharmacological evaluation as α 2-adrenoceptor ligands of O-phenylisouronium salts, *Bioorg. Med. Chem.* 16 (2008) 8210–8217.
- [20] For example: J.A. Platts, H. Maarof, K.D.M. Harris, G.K. Lim, D.J. Willock, The effect of intermolecular hydrogen bonding on the planarity of amides *Phys. Chem. Chem. Phys.* 14 (2012) 11944–11952. P. Prieto, A. De la Hoz, I. Alkorta, I. Rozas, J. Elguero, Strained π -systems as hydrogen bond acceptors: The case of benzyne, *Chem. Phys. Lett.* 350(2001) 325–330. I. Rozas, I. Alkorta, J. Elguero, The behaviour of ylides containing N, O, and C atoms, as hydrogen bond acceptors, *J. Am. Chem. Soc.* 122 (2000) 11154–11161.
- [21] For example: J.E. Rice, T.J. Lee, N.C. Handy, The analytic gradient for the coupled pair functional method: formula and application for HCl, H₂CO, and the dimer H₂CO...HCl, A. Nowek, J. Leszczyński, Ab initio investigation on stability and properties of XYCO...HZ complexes. II: Post Hartree-Fock studies on H₂CO...HF, *Struct. Chem.* 6(1995) 255–259. *J. Chem. Phys.* 88 (1988) 7011.
- [22] M. Head-Gordon, J.A. Pople, M.J. Frisch, MP2 energy evaluation by direct methods, *Chem. Phys. Lett.* 153 (1988) 503–506.
- [23] J. Tomasi, B. Mennucci, R. Cammi, Quantum mechanical continuum solvation models, *Chem. Rev.* 105 (2005) 2999–3093.
- [24] For example: M.T. Blazquez-Sanchez, F. Marcelo, M.C. Fernandez-Alonso, A. Poveda, J. Jimenez-Barbero, C. Vicent, Cooperative hydrogen bonding in glyco-oligoamides: DNA minor groove binders in aqueous media *Chem. Eur. J.* 20 (2014) 17640–17652. A. T. Lo, N. K. Salam, D. E. Hibbs, P. J. Rutledge, M. H. Todd, Polyamide-scorpion cyclam lexitropsins selectively bind AT-rich DNA independently of the nature of the coordinated metal, *PLoS One.* 6 (2011) e17446.
- [25] G.K. Kinsella, F. Rodriguez, G.W. Watson, I. Rozas, Computational approach to the basicity of a series of α 1-adrenoceptor ligands in aqueous solution, *Bioorg. Med. Chem.* 15 (2007) 2850–2855.
- [26] P.S. Nagle, A. Kahvedžić, T. McCabe, I. Rozas, On the protonated state of amidinium-like diaromatic derivatives: X-Ray and UV Studies, *Struct. Chem.* (2011) 1–9.
- [27] R. Williams "pKa Data compiled" (research.chem.psu.edu/brpgrp/pKa_compilation.pdf): A. Albert, R. Goldacre, J. Phillips, The strength of heterocyclic bases *J. Chem. Soc.* (1948) 2240–2249.
- [28] Marvin 14.10.6, Calculator Plugins Were Used for Structure Property Prediction and Calculation, ChemAxon, 2014, <http://www.chemaxon.com>.
- [29] Y. Zhao, D.G. Truhlar, The M06 suite of density functionals for main group thermochemistry, thermochemical kinetics, noncovalent interactions, excited states, and transition elements: two new functionals and systematic testing of four M06-class functionals and 12 other functionals, *Theor. Chem. Acc.* 120 (2006) 215.
- [30] (a) A.D. McLean, G.S. Chandler, Contracted Gaussian basis sets for molecular calculations. I. Second row atoms, Z=11–18, *J. Chem. Phys.* 72 (1980) 5639–5648; (b) R. Krishnan, J.S. Binkley, R. Seeger, J.A. Pople, Self-consistent molecular orbital methods. XX. A basis set for correlated wave functions, *J. Chem. Phys.* 72 (1980) 650–654; (c) T. Clark, J. Chandrasekhar, G.W. Spitznagel, P.v.R. Schleyer, Efficient diffuse function-augmented basis sets for anion calculations. III. The 3-21+G basis set for first-row elements, Li–F, *J. Comp. Chem.* 4 (1983) 294–301; (d) M.J. Frisch, J.A. Pople, J.S. Binkley, Self-Consistent molecular orbital methods 25: supplementary functions for Gaussian basis sets, *J. Chem. Phys.* 80 (1984) 3265–3269.
- [31] R.F.W. Bader, *Atoms in Molecules: a Quantum Theory*, Clarendon Press, Oxford, UK, 1990.
- [32] P.S. Neidle, DNA minor-groove recognition by small molecules, *Nat. Prod. Rep.* 18 (2001) 291–309.
- [33] C.H. Rohrig, C. Loch, J.Y. Guan, G. Siegal, M. Overhand, Fragment-based synthesis and SAR of modified FKBP ligands: influence of different linking on binding affinity, *ChemMedChem* 2 (2007) 1054–1070.
- [34] C. Dardonville, P. Goya, I. Rozas, A. Alsasua, I. Martin, M.J. Borrego, New aromatic iminoimidazolide derivatives as α 1-adrenoceptor antagonists: a novel synthetic approach and pharmacological activity, *Bioorg. Med. Chem.* 8 (2000) 1567–1577.
- [35] B. Nguyen, S. Neidle, W.D. Wilson, A role for water molecules in DNA-ligand minor groove recognition, *Acc. Chem. Res.* 42 (2009) 11–21.
- [36] V.J. Stella, *Prodrugs: Challenges and Rewards Part 1*, vol. 1, Springer, 2007.
- [37] B.J. Berger, R.J. Lombardy, G.D. Marbury, C.A. Bell, C.C. Dykstra, J.E. Hall, R.R. Tidwell, Metabolic N-hydroxylation of pentamidine in vitro, *Antimicrob. Agents. Chemother.* 34 (1990) 1678–1684.
- [38] Y. Hiraku, S. Oikawa, S. Kawanishi, Distamycin A, a minor groove binder, changes enediyl-induced DNA cleavage sites and enhances apoptosis, *Nucleic Acids Res.* 2 (2002) 95–96.
- [39] A. Lansiaux, L. Dassonneville, M. Facompre, A. Kumar, C.E. Stephens, M. Bajic, F. Tanious, W.D. Wilson, D.W. Boykin, C. Bailly, Distribution of furamide analogues in tumor cells: influence of the number of positive charges, *J. Med. Chem.* 45 (2002) 1994–2002.
- [40] A. Lansiaux, F. Tanious, Z. Mishal, L. Dassonneville, A. Kumar, C.E. Stephens, Q. Hu, W.D. Wilson, D.W. Boykin, C. Bailly, Distribution of furamide analogues in tumor cells: targeting of the nucleus or mitochondria depending on the amide substitution, *Cancer Res.* 62 (2002) 7219–7229.
- [41] X. Wu, F. Kassie, V. Mersch-Sundermann, Induction of apoptosis in tumor cells by naturally occurring sulfur-containing compounds, *Mutat. Res.* 589 (2005) 81–102.
- [42] D. Xiao, J.T. Pinto, G.G. Gundersen, I.B. Weinstein, Effects of a series of organosulfur compounds on mitotic arrest and induction of apoptosis in colon cancer cells, *Mol. Cancer Ther.* 4 (2005) 1388–1398.
- [43] J. Lennon, S.A. Bright, E. Carroll, S. Butini, G. Campiani, A. O'Meara, D.C. Williams, D.M. Zisterer, The novel pyrrolo-1,5-benzoxazepine, PBOX-6, synergistically enhances the apoptotic effects of carboplatin in drug sensitive and multidrug resistant neuroblastoma cells, *Biochem. Pharmacol.* 87 (2014) 611–624.
- [44] M. Bataller, C. Mendez, J.A. Salas, J. Portugal, Mithramycin SK modulates ploidy and cell death in colon carcinoma cells, *Mol. Cancer Ther.* 7 (2008) 2988–2997.
- [45] R.S. DiPaola, To arrest or not to G2-M cell-cycle arrest, *Clin. Cancer Res.* 8 (2002) 3311–3314.
- [46] K. Wassmann, R. Benezra, Mitotic checkpoints: from yeast to cancer, *Curr. Opin. Genet. Dev.* 1 (2001) 83–90.
- [47] M.J. Frisch, G.W. Trucks, H.B. Schlegel, G.E. Scuseria, M.A. Robb, J.R. Cheeseman, G. Scalmani, V. Barone, B. Mennucci, G.A. Petersson, H. Nakatsuji, M. Caricato, X. Li, H.P. Hratchian, A.F. Izmaylov, J. Bloino, G. Zheng, J.L. Sonnenberg, M. Hada, M. Ehara, K. Toyota, R. Fukuda, J. Hasegawa, M. Ishida, T. Nakajima, Y. Honda, O. Kitao, H. Nakai, T. Vreven, J.A. Montgomery, F. Ogliaro, M. Bearpark, J.J. Heyd, E. Brothers, K.N. Kudin, V.N. Staroverov, R. Kobayashi, J. Normand, K. Raghavachari, A. Rendell, J.C. Burant, S.S. Iyengar, J. Tomasi, M. Cossi, N. Rega, N.J. Millam, M. Klene, J.E. Knox, J.B. Cross, V. Bakken, C. Adamo, J. Jaramillo, R. Gomperts, R.E. Stratmann, O. Yazyev, A.J. Austin, R. Cammi, C. Pomelli, J.W. Ochterski, R.L. Martin, K. Morokuma, V.G. Zakrzewski, G.A. Voth, P. Salvador, J.J. Dannenberg, S. Dapprich, A.D. Daniels, Ö. Farkas, J.B. Foresman, J.V. Ortiz, J. Cioslowski, D.J. Fox, Gaussian 09, Revision A.02, Gaussian, Inc., Wallingford, CT, 2009.
- [48] D.J. Brennan, J.E. White, A.P. Haag, S.L. Kram, M.N. Mang, S. Pikulin, C.N. Brown, Poly(hydroxy amide ethers): new high-barrier thermoplastics, *Macromolecules.* 29 (1996) 3707–3716.